Oxoeicosanoid signaling mediates early antimicrobial defense in zebrafish

Yanan Ma[1], **King Lam Hui**[1], **Zaza Gelashvili**[1,2], **Philipp Niethammer**[1,3,*]

[1]Cell Biology Program, Memorial Sloan Kettering Cancer Center, New York, NY 10065, USA

[2]Gerstner Sloan Kettering Graduate School of Biomedical Sciences, New York, NY 10065, USA

[3]Lead contact

SUMMARY

5-oxoETE is a bioactive lipid derived from arachidonic acid generated when phospholipase A_2 activation coincides with oxidative stress. Through its G protein-coupled receptor OXER1, pure 5-oxoETE is a potent leukocyte chemoattractant. Yet, its physiological function has remained elusive owing to the unusual *OXER1* conservation pattern. *OXER1* is conserved from fish to primates but not in rodents, precluding genetic loss-of-function studies in mouse. To determine its physiological role, we combine transcriptomic, lipidomic, and intravital imaging assays with genetic perturbations of the *OXER1* ortholog *hcar1–4* in zebrafish. *Pseudomonas aeruginosa* infection induces the synthesis of 5-oxoETE and its receptor, along with other inflammatory pathways. *Hcar1–4* deletion attenuates neutrophil recruitment and decreases post-infection survival, which could be rescued by ectopic expression of *hcar1–4* or human *OXER1*. By revealing 5-oxoETE as dominant lipid regulator of the early antimicrobial response in a non-rodent vertebrate, our work expands the current, rodent-centric view of early inflammation.

In brief

5-oxoETE is an inflammatory lipid derived from arachidonic acid. 5-oxoETE's physiological functions are little understood, partly because its G protein-coupled receptor, OXER1, has no known rodent orthologs. Here, Ma et al. use zebrafish, which express OXER1 orthologs, to illuminate the pathway's essential physiological functions in rapid innate immune defense against bacterial infection.

Graphical Abstract

*Correspondence: niethamp@mskcc.org.

INTRODUCTION

Arachidonic acid (AA)-derived metabolites are a large family of signaling lipids termed eicosanoids. They have essential roles in cell-to-cell communication during inflammation and innate immune defense. Drugs that target eicosanoid signaling are among the most prescribed of any medicines, but innovation has largely ceased in recent years. This could reflect that eicosanoid biology is already completely understood and therapeutically exploited. Or it may reflect an over-reliance on rodent models that do not always accurately predict human pathophysiology.[1,2] Many of the synthesis routes, receptor mechanisms, and physiological roles of eicosanoids remain little characterized. A prime example is 5-oxoETE (5-oxo-6E,8Z,11Z,14Z-eicosatetraenoic acid, also called 5-oxoETE), which is derived from AA by the action of 5-lipoxygenase (ALOX5) and the genetically unidentified enzyme 5-hydroxyeicosanoid dehydrogenase (5-HEDH), or by non-enzymatic lipid peroxidation.[3] Like the well-studied neutrophil chemoattractant leukotriene B4 (LTB$_4$), which is generated from AA by ALOX5 and leukotriene A4 hydrolase (LTA$_4$H), pure 5-oxoETE attracts leukocytes, most potently eosinophils.[4] Ischemic or allergic challenge elevates 5-oxoETE levels *in vivo*.[5,6] Pharmacologic antagonism of OXER1 alleviates allergic inflammation in monkey.[7,8] In human cancers, the *OXER1* gene shows a frequent frameshift mutation (S78Pfs*64 and S78Vfs*61).[9] Cell culture studies reported 5-oxoETE to act proliferative or antiproliferative depending on concentration.[10,11] In any case, whether or how tumorigenesis is influenced by OXER1 is hard to predict without knowing the receptor's physiological

function. In zebrafish, morpholino-mediated knockdown of the *OXER1* ortholog *hcar1–4* inhibits neutrophil recruitment to uninfected tail fin wounds.[12] Since those usually heal rapidly without impairing larval survival, they do not exert enough selective pressure to reveal the broader importance of oxoeicosanoid signaling during immune defense. To this end, we set out to illuminate the role of oxoeicosanoid signaling in a zebrafish infection model.

RESULTS

For studying innate immunity, transparent zebrafish larvae are a powerful alternative to mice.[13] All major innate immune cell types are present in zebrafish.[14] Owing to the thinness and translucency of zebrafish larvae, they can be conveniently studied *in situ* by intravital imaging. Along with many other human genes (including CASP10, ADA2, etc.), OXER1 has no described orthologs in mouse or rat, but in fish (Figures 1A and S1A; Table S1). As pure 5-oxoETE and chemical OXER1 antagonists also show effects on rodents,[15–19] there might be unknown OXER1 substitutes. But until those are found—given they exist—the oxoeicosanoid pathway cannot be interrogated using mouse genetics.

According to the ENSEMBL database (release 107), there are 206 not-rat-nor-mouse (NRNM) genes (Table S1), defined here as zebrafish genes conserved in human and cat but not in rat or mouse. This list includes some genes with known rodent homologs, such as the high-affinity LTB$_4$ receptor (BLT1) and others. We used the DIOPT[20] metasearch engine (version 9.0, Sept 2021) to filter out such potential false positives, which left us with 153 likely NRNM genes (Table S1). For illuminating their physiological roles, the zebrafish model is a compelling choice, because intravital imaging and genetic loss-of-function studies are prohibitively challenging in most non-rodent mammals.

Fluorescence-activated cell sorting (FACS) of dissociated leukocyte reporter larvae and quantitative RT-PCR (qRT-PCR) confirmed that the transcripts of the two zebrafish orthologs, *hcar1–3* and *hcar1–4,* are enriched in neutrophils (Figure 1B).[12,21] Unlike *hcar1–4*, *hcar1–3* mRNA is also highly enriched in macrophages. To profile early transcriptional responses to infection, we performed mRNA sequencing (mRNAseq) of larvae before and 2 and 4 h after injection of *Pseudomonas aeruginosa* (PA) into the otic vesicle of 3 days post fertilization (dpf) zebrafish larvae as previously described (Figure 1C).[22–24] The mRNAseq expression profiles were sorted by their correlation distance to all possible binary gene expression phenotypes by a novel gene correlation analysis method we developed for this study (Figure S1B, Table S2, first tab). Our *simple Gene Correlation Analysis* (sGCA) does not cluster gene expression profiles by their mutual correlation as other, unbiased clustering methods, but by their similarity to binary, "ideal phenotypes" (IPs, i.e., logical gates) defined by the experimental groups (Figure S1B). sGCA associated *hcar1–4* with the largest inflammatory cluster (IP60), which comprises genes maximally induced at 4 h post infection (Figure 1C, Table S2, second and third tab). By its highest-ranking gene ontology terms, functional profiling classifies the IP60 cluster as "immune system process" and "defense response" (Table S2, fourth tab). Functional profiling results for all IP clusters are listed in Table S2. The time course of *hcar1–4* expression upon infection is reminiscent of known immune genes, including *cxcr1* (GPCR for interleukin 8) and *ltb4r*, *ltb4r2a* and *ltb4r2b*

(high- and low-affinity GPCRs for LTB$_4$) (Figure 1C, inset). Whereas *hcar1–3* was hardly detectable by mRNAseq, qRT-PCR indicated its modest induction upon infection (Figure S1C). To test whether Hcar1–4 regulates inflammatory gene transcription, we generated two *hcar1–4* mutant alleles (*hcar1–4^{mk213}* and *hcar1–4^{mk214}*) using CRISPR-Cas9 (Figures S1D and S1E). IP21 and IP42 include genes either significantly induced or suppressed by *hcar1–4* mutation. Although some of those genes are immune related, we did not detect significant inflammatory signatures by functional profiling. *Hcar1–4* may be more a target than a regulator of inflammatory gene transcription. The zebrafish mucin *mucms1* (567x down, P21) and caspase 6 (*casp6a*, 167x up, P42) are the most regulated genes in these IP clusters (Figure 1C, Table S2, second and third tab). Interestingly, pharmacologic OXER1 inhibition in monkeys was shown to decrease the number of mucus-producing cells in the bronchial epithelium,[8] consistent with additional, non-inflammatory functions of the OXER1 pathway in mucosal homeostasis.

To test whether microbial infection gives rise to physiologically relevant concentrations of 5-oxoETE, we conducted liquid chromatography coupled mass spectroscopic analysis of infected zebrafish larvae at the UC San Diego LIPIDMAPS facility.[25] The baseline concentrations of the 78 detected lipid species showed considerable differences, with the 5-oxoETE precursor 5-HETE being among the most abundant and significantly induced species. Whereas the baseline of this and other oxidized fatty acid derivatives may include contributions of passive sample oxidation, the baseline-corrected, infection-induced concentration changes are likely of biological origin. 5-oxoETE, but not LTB$_4$, showed a strong and significant infection-induced ~2 μM increase over baseline (Figure 1D). According to earlier studies,[12,26] this concentration range is optimal for attracting neutrophils *in vitro* and *in vivo.*

We next asked whether the OXER1 pathway conveys any relevant antimicrobial protection. Indeed, control of microbial growth and post-infection survival of *hcar1–4* mutants were significantly reduced compared with wild-type (WT) sibling controls (Figures 2A–2C and S2A), yet rescued by ectopic expression of human OXER1 or Hcar1–4 fused with red fluorescent protein (mKate2, mk2) (Figures 2C and S2B). Since neutrophils are the main antimicrobial immune cell type in vertebrates, and because the observed 5-oxoETE levels are expected to mediate chemotaxis of human and zebrafish neutrophils,[12,26] the reduced post-infection survival may be, at least in part, caused by a decrease in neutrophil recruitment. In line with earlier experiments using zebrafish tail fins,[12] exposure to pure 5-oxoETE triggered significant neutrophil migration to infected ears in WT but not in *hcar1–4^{mk214}* mutant larvae under isotonic bathing conditions that block the endogenous release of AA-derived chemoattractants[12,24,27] (Figure 2D). Importantly, Sudan black-staining revealed a pronounced decrease in neutrophil recruitment to the infected ears of *hcar1–4* mutants under normal (hypotonic) infection conditions (Figures 2E, S2C, and S2D). At the same time, overall neutrophil counts between WT and mutant animals remained about the same (Figures S2E and S2F). Furthermore, after systematically infecting larvae by PA injection into the common cardinal vein/duct of Cuvier (CCV/DC),[28] animal survival and neutrophil numbers in the caudal hematopoietic tissue (CHT) were significantly reduced in *hcar1–4$^{mk213\ -/-}$* but not WT larvae (Figures S2G–S2J). It remains to be delineated whether these latter observations reflect defects in leukocyte chemotaxis, degranulation, survival, or

all the above. Collectively, our results suggest that 5-oxoETE/OXER1 signaling is broadly involved in infection defense.

To monitor early leukocyte recruitment to infected ears *in situ*, we introduced *hcar1–4* and *hcar1–3* F0 CRISPR mutations into fluorescent leukocyte reporter lines[29,30] (Figures 2F, S2K–S2P, S3A–S3C). Live imaging confirmed that leukocyte infiltration into the ear region of *hcar1–4*, but not *hcar1–3*, F0 CRISPR larvae became attenuated at ~1 h after infection (Figures 2F and S3A, Videos S1 and S2), while early macrophage recruitment was unaffected by mutation of either receptor (Figures S3B and S3C, Videos S3 and S4). Interestingly, after tail fin amputation, *hcar1–4* mutants (Figures S3D and S3E) and morphants[12] showed defective neutrophil recruitment during the first hour after injury, that is, earlier than observed for neutrophil recruitment to infected ears (Figure 2). Conceivably, this temporal offset might be caused by a limited availability of 5-oxoETE ligand or Hcar1–4 receptor during the first hour after infection. 5-oxoETE synthesis via 5-HEDH or non-enzymatic mechanisms is regulated by oxidative stress,[31,32] and redox differences between zebrafish tail fin wounds and infection sites that could impinge on delayed 5-oxoETE synthesis have been previously noted by others.[22] Likewise, it is possible that initially only a subpopulation of neutrophils (e.g., those in the CHT) expresses enough Hcar1–4 to immediately respond to 5-oxoETE, and that microbial pattern recognition through Toll-like receptors (TLRs) is required for a more uniform if delayed responsiveness to 5-oxoETE. In line with this idea, knockdown of the TLR-adaptor molecule Myd88 by F0 CRISPR blunted the infection-induced *hcar1–4* expression (Figures 1C and 2G). To further explore *hcar1–4's* relationship with microbial pattern recognition, we perturbed Toll- and NOD-like receptor signaling by CRISPR F0 of *myd88* and *pycard*[33,34] both in WT and *hcar1–4^{mk214 –/–}* animals (Figures S4A–S4F): *myd88*, *pycard*, and *hcar1–4* mutation all caused similar neutrophil recruitment defects (Figures 3A and 3B), which were, however, not further aggravated when *myd88* or *pycard* were mutated together with *hcar1–4*. This suggests that *hcar1–4*, *myd88*, and *pycard* are part of a pathway, in which microbial pattern recognition stimulates *hcar1–4* expression.

To compare the relative chemotactic role of 5-oxoETE-OXER1 during the early infection response to LTB$_4$—one of the most studied chemotactic lipid pathways to date—we mutated *lta4h* and *ltb4r* using F0 CRISPR in WT and *hcar1–4^{mk214 –/–}* animals (Figures S4G–S4L). Through its high-affinity receptor Ltb4r (BLT1), LTB$_4$ acts as a chemotactic relay signal during neutrophil swarming in mouse and zebrafish.[35–37] However, we did not observe a significant neutrophil recruitment defect of *ltb4h* or *ltb4r* mutants, alone or in combination with *hcar1–4* mutation, within 2 h after ear infection (Figures 3C and 3D). Whereas BLT1 gene deletion in mouse attenuates neutrophil swarming to dermal ear wound sites as early as ~30 min after injury,[35] our data and previous studies provide little support for such immediate effect in zebrafish.[12,37,38] As of 2017, most reported clinical trials targeting the LTB$_4$ pathway were unsuccessful,[39] leaving its precise pathophysiological role in humans largely undefined.

DISCUSSION

Several possible explanations for the species-dependent differences in inflammatory LTB_4 signaling (Figure 4) deserve further investigation. For one, in animals that lack OXER1, its function during early inflammation might have been replaced by other receptors, such as BLT1. An entanglement of NRNM genes, such as OXER1, in inflammatory gene circuits could explain at least some of the long-noted differences between human and mouse inflammatory programs.[1,2] Although rodents are often a better proxy for human biology than fish, for example, when studying mammalian reproduction, our work suggests that the opposite case can also apply. This highlights a perhaps less obvious and little exploited strength of the zebrafish model: using zebrafish to target blind spots of mouse genetics can illuminate the physiological and pathophysiological functions of genetically otherwise inaccessible, inflammatory mechanisms as previously shown for human adenosine deaminase 2 (ADA2)[40] and now for OXER1.

Limitations of the study

Hcar1–4 is broadly expressed in various tissues besides leukocytes. Our current work does not address potential tissue specific functions of the receptor; that is, it does not formally distinguish how myeloid and epithelial functions of Hcar1–4 contribute to the observed phenotypes. The F0 CRISPR approaches used here may underestimate the effects of a full (i.e., non-mosaic), homozygous gene mutation. The CCV infection experiment does not delineate the precise cellular mechanism (defect in chemotaxis, leukocyte survival, or degranulation, etc.) by which Hcar1–4 loss causes the observed phenotypes (survival defect, decreased Sudan black-staining). Our data do not formally exclude that structurally related lipids, such as 5-oxo-EPE (not measured here), are also ligands for Hcar1–4.

STAR★METHODS

RESOURCE AVAILABILITY

Lead contact—Further information and requests for resources and reagents should be directed to and will be fulfilled by the lead contact, Philipp Niethammer (NiethamP@mskcc.org).

Materials availability—All unique/stable reagents generated in this study are available from the lead contact with a completed Materials Transfer Agreement.

Data and code availability

- RNA-sequencing data are available at the GEO data depository under number GSE201604. This accession number is also listed in the key resources table.

- All original code has been deposited at Zenodo and is publicly available as of the date of publication. DOI (https://doi.org/10.5281/zenodo.7419586) is also listed in the key resources table. The sGCA script and MATLAB app are also available on GitHub (https://github.com/niethamp/sGCA-Ma-et-al.-2022-).

- Any additional information required to reanalyze the data reported in this paper is available from the lead contact upon request.

EXPERIMENTAL MODEL AND SUBJECT DETAILS

General fish procedures—Adult wt and transgenic reporter *casper*[41] zebrafish were maintained at the Memorial Sloan Kettering Cancer Center (MSKCC) Zebrafish Core Facility[43] and subjected to experiments according to institutional animal healthcare guidelines with the approval of the Institutional Animal Care and Use Committee (IACUC) of MSKCC. For injection and wounding assays, 2.5–3 days post-fertilization (2.5–3 dpf) larvae were anesthetized in standard hypotonic E3 medium (5 mM NaCl, 0.17 mM KCl, 0.33 mM $CaCl_2$, 0.33 mM $MgSO_4$) containing 0.2 mg/mL ethyl 3-aminobenzoate methanesulfonate (Tricaine/Syncaine, Sigma, E10521). For the 2.5–3 dpf zebrafish larvae used in this study, sex cannot be determined and is unlikely to influence the biological processes under study.

METHOD DETAILS

Bacterial strains and growth conditions—The wild-type (*wt*) *Pseudomonas aeruginosa* (strain PA14) used here was originally provided by Dr. Joao Xavier (MSKCC, New York, NY).[24] PA14 were grown in lysogeny broth (LB) medium. To prepare the final inoculum, the bacteria suspension was diluted or pelleted to achieve the desired bacterial density (OD_{600} = 7).

Bacterial infection through ear (local) or common cardinal vein/duct of cuvier (CCV/DC) (systemic) injection—PA ear injection was performed as follows[24]: Fluorescent beads, blue-green (Cyan) (Ex/Em = 430/465) (Thermo Fisher, F13080) or Red (Ex/Em = 580/605) (Thermo Fisher, F8810) FluoSphere were mixed 1:1 with bacterial suspensions prior to injection. 1 μM 5-oxoETE (Cayman, cat#34250) in dimethyl sulfoxide (DMSO, Sigma, D8418) was mixed with PA in isotonic E3 (standard E3 + 140 mM NaCl) and injected into the otic vesicle (i.e., ear) of larvae. CCV/DC injection was conducted with 2.3 nL PA14 (OD_{600} = 7),[44] dextran (Invitrogen, D7136) which was dissolved in 1× phosphate buffered saline (PBS, Sigma, 79,382) at concentration of 1 mg/mL was used to monitor success of CCV/DC injection. We performed ear and CCV/DC injections with ~2 × 10^4 CFU per injection.

Tail fin amputation—For wounding experiments, the tail fin tips of anesthetized 2.5–3 dpf larvae were removed with a surgical microblade (Fine Science Tools, 10,318) at the boundary of the notochord without injuring the notochord.[45]

Sudan-black staining—To visualize neutrophil recruitment, larvae were fixed at indicated times after wounding or ear infection using 4% formaldehyde in 1× PBS overnight at 4°C, and then stained with Sudan-black for 30 min. The stained zebrafish larvae were washed three times in 70% ethanol followed by rehydration with PBST for 5 min. Finally, the larvae were washed with depigmentation solution (10% KOH, 30% H_2O_2) and twice in PBST prior to imaging.[46]

Generation of *hcar1–4* mutant lines and genotyping—Four independent gRNAs (*hcar1–4*-sgRNA-1, *hcar1–4*-sgRNA-2, *hcar1–4*-sgRNA-3, *hcar1–4*-sgRNA-4) of *hcar1–4* (ENSDARG0000 0087084) were designed and ordered from IDT (Integrated DNA Technologies). The Cas9-gRNA (single *hcar1–4*-sgRNA-1 or four *hcar1–4*-sgRNA-1, *hcar1–4*-sgRNA-2, *hcar1–4*-sgRNA-3, *hcar1–4*-sgRNA-4) ribonucleoprotein complex solution was injected into the cytoplasm of one-cell-stage zebrafish embryos. After the injected F0 larvae had been grown to sexual maturity (2–3 months post-fertilization), individual F0 adults were crossed to wild-type adults to get F1 progeny. These F1 larvae were then grown to sexual maturity, and genomic DNA was isolated from their tailfins for genotyping. To this end, the tailfins were partially amputated and suspended in 250 μL of 50 mM NaOH, and then incubated at 95°C for 10 min. Then, samples were cooled on ice for 10 min, neutralized with 25 μL of 1M Tris-HCl (pH 8) and vortexed. The genotyping primers are listed in Table S3. PCR products from F1 *hcar1–4*-sgRNA-1 adult fish were incubated with FastDigest BstXI (Thermo Fisher Scientific; FD1024) enzyme at 37°C overnight, and the reaction mixture was separated by agarose gel electrophoresis. F1 heterozygous adults were identified by the presence of three DNA fragments (~422, 269 and 153 bp). The ~422 bp product represents a mutant allele for which the BstXI site has been destroyed by Cas9-induced mutation. The ~422 bp band was isolated from agarose and sequenced by Sanger sequencing. The F1 heterozygous adult zebrafish with the frameshiftmutation of interest (11 bp insertion, *hcar1–4*^{mk213}, Figure S1) were crossed to homozygosity. PCR products from F1 *hcar1–4*-sgRNA-1, *hcar1–4*-sgRNA-2, *hcar1–4*-sgRNA-3 and *hcar1–4*-sgRNA-4 heterozygous adult zebrafish were separated by agarose gel electrophoresis. The F1 heterozygous adult zebrafish with the large truncation of interest (313 bp, *hcar1–4*^{mk214}, Figure S1) were crossed to get F2 homozygous mutant *hcar1–4*^{mk214} progeny.

F0 CRISPR gene perturbation approach—Potential gRNA target sites were identified using the web program CHOPCHOP (http://chopchop.cbu.no/index.php). All gRNA target sequences are listed in STAR Methods. Three independent gRNAs for *hcar1–4* (ENSDARG00000087084), *myd88* (ENSDARG00000010169), *pycard* (ENSDARG00000040076), *ltb4r* (ENSDARG00000032631), and four independent gRNAs for *hcar1–3* (ENSDARG00000062874), and *lta4h* (ENSDARG00000006029) were designed and ordered from IDT. These target-specific Alt-R™ crRNA (Crispr RNA) and common Alt-R tracrRNA (Trans-Activating Crispr RNA) were dissolved in nuclease-free duplex buffer (IDT; 11–01-03–01) to yield a 100 μM stock solution. To prepare the crRNA:tracrRNA duplex, equal volumes of 100 μM Alt-R crRNAs (1:1:1:1 or 1:1:1) and 100 μM Alt-R tracrRNA stock solutions were mixed with nuclease-free duplex buffer to a final concentration of 10 μM each. The mixture was subsequently heated to 95°C for 5 min, and then cooled down to room temperature. ALT-R S.p. Cas9 Nuclease (IDT, 1081058) was diluted to 1 mg/mL with Cas9 working buffer (20 mM HEPES, 150 mM KCl, pH 7.5). The Cas9-gRNAs ribonucleoprotein complex was assembled by combining the crRNA:tracrRNA duplex and Cas9 protein solutions as 1:1 (vol/vol). Prior to microinjection, the Cas9-gRNAs ribonucleoprotein complex solution was incubated at 37°C for 5 min and placed at room temperature. Approximately 2.3 nL of the Cas9-gRNAs ribonucleoprotein complex solution was injected into the cytoplasm of one-cell-stage zebrafish embryos. At 2.5–3 dpf, genomic DNA was isolated from 18 individual F0 larvae for genotyping. Briefly, 50 μL of 50 mM

NaOH was added to each larvae and incubated at 95°C for 10 min, subsequently, the genomic DNA was placed on ice and 5 μL of 1 M Tris-HCl (pH 8.0) was added.[47] Each specific target sequence of interest was PCR amplified from the genomic DNA samples with the primers listed in Table S3. Next, PCR products were incubated with the FastDigest restriction enzymes (BstXI for *hcar1–4*-sgRNA-1 product, BseLI for *hcar1–4*-sgRNA-5 product, MseI for *hcar1–4*-sgRNA-6 product; BseNI for *hcar1–3*-sgRNA-1 product, BseLI for *hcar1–3*-sgRNA-2 product, HpaII for *hcar1–3*-sgRNA-3 product, Eco47I for *hcar1–3*-sgRNA-4 product; BseNI for *myd88*-sgRNA-1, OliI for *myd88*-sgRNA-2, BseLI for *myd88*-sgRNA-3; PvuI for *pycard*-sgRNA-1, Bsp1286I for *pycard*-sgRNA-2, SmlI for *pycard*-sgRNA-3; BseLI for *lta4h*-sgRNA-1, BseLI for *lta4h*-sgRNA-2, SalI for *lta4h*-sgRNA-3, BstXI for *lta4h*-sgRNA-4; BseLI for *ltb4r*-sgRNA-1, BseLI for *ltb4r*-sgRNA-2, BstXI for *ltb4r*-sgRNA-3) for at least 2 h at 37°C. Then, samples were separated by agarose gel electrophoresis (Table S4).

Survival assays—Survival after ear infection, and survival after CCV/DC systemic infection were performed as follows. 2.5–3 dpf larvae were infected with PA in standard hypotonic E3 either in the ear or in the CCV/DC. Then, infected larvae were placed into the wells of a 48-well plate, and their viability was monitored for 5 days after injection. Dead larvae were scored by loss of transparency and heartbeat.

Colony forming units (CFU) assay—CFUs of infected, 2.5–3 dpf zebrafish larvae were measured as follows[48]: In brief, at 2 h or 4 h post-infection, a total of 40 larvae were distributed into eight groups (5 larvae per group) in 1.5 mL Eppendorf tubes. The infected larvae were washed three times with PBS to remove adherent bacteria. The larvae were homogenized in filter-sterilized PBS with 1% Triton X-100 (Sigma, SLBW7103) (40 μL per larvae). The suspension was diluted to 1:100, and 10 μL was plated onto LB agar plates, then incubated overnight at 37°C. We inferred the bacterial burden of the infected larvae by colony counting of LB plates.

Spinning disk confocal imaging—For live imaging, anesthetized TG(*lyz*:pm2-mk2)[42] or TG(*mpeg1*:eGFP)[42] 2.5–3 dpf larvae were injected with PA mixed with fluorescent cyan or red beads to mark the ear region. The larvae were then immobilized by embedding them in ~200 μL of 1% low-melting agarose (Gold Biotechnology, A-204–100) dissolved in standard hypotonic E3 in glass bottom dishes (MatTek Corporation, P35G-1.5–20-C). After the agar had solidified, the mounted larvae were covered with 2–3 mL E3-Tricaine to prevent desiccation and maintain anesthesia during imaging.

Imaging was performed at 28°C in heated imaging chamber (TOKAI HTI, WPI inc.) on an inverted Nikon Eclipse Ti microscope equipped with a CFI Plan Apochromat Lambda D 10× Objective lens (NA 0.45), a motorized stage, a Yokogawa CSU-W1 Spinning Disk unit, a Photometrics Prime BSI Scientific CMOS camera (2×2 binning), and NIS imaging software (Nikon, 5.11.01). Fluorescence emission was excited using 405, 488 or 561 nm diode lasers (Nikon). Channel acquisition intensities/exposure times used in the study were as follows: 80%/100 ms (561 nm) or 50%/100 ms (488 nm) laser power settings were used to detect either neutrophils or macrophages. The injected red (E_x/E_m: 580/605) or cyan (E_x/E_m: 430/465) fluorescent polystyrene beads were excited by adjusting laser power to

30%/100 ms (561 nm) or 40%/100 ms (405 nm), respectively. The emission was collected using 455/50 (cyan), 525/36 (green) or 605/52 (red) bandpass filters.

Image processing and data analysis—The acquired confocal z-stacks were imported into Imaris (Bitplane, 9.6.0) for counting the leukocytes in the ear region over time. To this end, we constructed a 3D region of interest (390 μm × 390 μm × 100 μm) by manually marking the center of the ear (based on bead fluorescence) using the Imaris wand tool. The Imaris spot detection and wizard filter tools were used to remove non-specific signals for manual 3D-segmentation and quantification of leukocytes based on size (~13 μm diameter) or fluorescence signal intensity threshold filters that were manually adjusted for emission quality and quantified.

mRNA preparation and injection—For the zebrafish *hcar1–4* or human *OXER1* rescue experiments, pCS2+*hcar1–4*-mKate2 or pCS2+OXER1-mKate2 were linearized using FastDigest NotI (Thermo Fisher Scientific; FD0593), and *in vitro* transcribed using the mMessage mMachine SP6 kit (Thermo Fisher Scientific; AM1340). 2.3 nL of ~500 ng/μL mRNA was injected into the yolk of one-cell stage zebrafish embryos.

Cell sorting and quantitative RT-PCR—2.5–3 dpf larvae (n~400) were collected from TG(*lyz*:pm2-mKate2) or TG(*mpeg1*:eGFP) transgenic lines expressing red (mKate2) or green (eGFP) fluorescent protein in neutrophils or macrophages, respectively. Larvae were dissociated into a single cell suspension as follows[49]: Cell sorting and collection of eGFP or mKate2 positive and negative cells was carried out by FACS (Aria, BD Bioscience) based on 561 nm excitation and 670/30 nm emission wavelengths for mKate2 and 488 nm excitation and 525/50 nm emission for GFP.

mRNA was isolated using the RNeasy Plus Micro kit (QIAGEN; 74,034), cDNA was prepared using the High-Capacity cDNA Reverse Transcription kit (Thermo Fisher Scientific; cat#4368814), and quantitative RT-PCR was carried out using the Maxima SYBR Green/Fluorescein qPCR Master Mix (Thermo Fisher Scientific; K0242) on a Real-Time PCR Machine (Bio-Rad, Watford, Hertfordshire, UK) (Figure 1B). Data were normalized to β-actin using the $2^{-\Delta Ct}$ method.[50] Primer sequences are listed in Table S3.

Lipidomics analysis—2.5–3 dpf wt larvae (total ~1200, ~400 per replicate) were collected after PA ear injection at 2 h. Uninfected wt larvae (total ~1200, ~400 for each sample) were collected as control and sent to the UC San Diego Lipid Maps facility for full eicosanoid panel chromatography/mass spec analysis. Zebrafish larvae were homogenized in 1 mL 10% methanol in water using a Bead Mill 24 (Fisher Scientific, 15–340-163). A mix of 26 deuterated internal standards was added to 100 μL homogenate. Eicosanoids were extracted by solid phase extraction (SPE) using Phenomenex Strata-X polymeric reversed phase columns. Samples were brought to dryness and taken up in buffer A (water/acetonitrile/acetic acid 60/40/0.02, v/v/v). Samples were analyzed using a Waters Acquity UPLC interfaced with an AB Sciex 6500 QTrap instrument. Chromatographic separation was achieved by a step gradient starting with 100% buffer A to 100% buffer B (acetonitrile/isopropanol 50/50, v/v) over 5 min. Standard curves were obtained in parallel using identical conditions. Data analysis was performed with Analyst and Mulitquant software packages.[25]

Embryo collection, RNA extraction, and sequencing—For the qRT-PCR in Figure S1C, 2.5–3 dpf wt larvae (every time point ~120, 40 for each sample) were collected after PA ear injection at 0 h, 1 h, 2 h, 4 h, 8 h, 12 h and 24 h. mRNA was isolated using Trizol reagent (Thermo Fisher Scientific; cat#15596026) according to the manufacturer's protocol. cDNA was prepared using the RevertAid First Strand cDNA Synthesis Kit (Thermo Fisher Scientific; K1621), and QPCR was carried out using the Maxima SYBR Green/Fluorescein qPCR Master Mix (Thermo Fisher Scientific; K0242). As for the mRNA-sequencing in Figures 1C, 2.5–3 dpf *hcar1–4*$^{mk213\,+/+}$ or *hcar1–4*$^{mk213\,-/-}$ larvae were collected after PA ear injection at 2 h and 4 h. Noninjected *hcar1–4*$^{mk213\,+/+}$ or *hcar1–4*$^{mk213\,-/-}$ larvae were used as a control. mRNA was extracted as described above. The following procedures were performed by the MSKCC Genomics and Bioinformatics core facilities as follows[24]: In brief, the RNA-seq libraries were sequenced on the Illumina HiSeq2500 platform with paired-end 50-bp single reads, resulting with an average of 20–30 million reads per sample. The sequence data (FASTQ files) were processed and mapped to the zebrafish genome GRCz11 (UCSC) using the rnaSTAR aligner that genomically mapped and resolved reads across splice junctions. The resulting SAM files were processed using the PICARD tools for conversion and compression of the output to the BAM file format. The mapped reads were then processed using DESeq, from R/BioConductor to analyze differential gene expression between samples. The mRNAseq data are available at https://www.ncbi.nlm.nih.gov/geo/query/acc.cgi?acc=GSE201604.

Ortholog analysis—Sequence orthologs (one2one or one2many or many2many) of zebrafish genes in human (*homo sapiens*), cat (*felis catus*), rat (*rattus norvegicus*), and mouse (*mus musculus*) were retrieved using BioMart and ENSEMBL release 107 (Jul 2022). A Venn diagram of these orthologs was generated with a webtool (https://bioinformatics.psb.ugent.be/webtools/Venn/) and displayed in Figure 1C. To remove likely false positives from the ENSMBL NRNM list (i.e., 206 zebrafish genes with ENSEMBL orthologs in human and cat but not mouse or rat), we used the DIOPT ortholog finder webtool (version 9.0, Sept 21, beta),[20] which searches across the Alliance of Genome Resources (AGR) databases with AGR-selected algorithms. False-positive NRNM genes were defined as genes that were assigned by ENSEMBL as NRNM genes yet had "high"-ranking DIOPT rat or mouse orthologs (Weighted score >2 & Rank = High & Best Score = Yes & Best Score Reverse = Yes). Those (n = 53; Table S1, tab four & five tab) putative false positives were removed from the original ENSEMBL NRNM list, leaving a final list of 153 likely NRNM genes (Table S1, second tab). 49 from this "cleaned" NRNM list had "high" ranking human orthologs according to the above DIOPT criteria.

Simple gene correlation analysis (sGCA)—sGCA calculates the correlation distance (CD, one minus the sample correlation between points treated as sequences of values, as per MATLAB definition) of all actual mRNAseq expression phenotypes to "ideal" phenotypes (IP). That is, CD = 0 means that an expression profile perfectly correlates with the respective IP, CD = 1 means the opposite. Once a gene has been assigned to an IP, its fold-regulation is calculated by dividing the mean of 1-group-conditions by the mean of the 0-group-conditions ("condition" = columns of normalized mRNAseq count matrix where rows denote the genes). The respective P_{adj} is calculated using a negative binomial model

with Benjamini-Hochberg adjustment. The mean base is calculated as the mean of means of 1-group-conditions and 0-group-conditions. The heatmap in Figure 1C only includes genes with CD < 0.25, P_{adj} < 0.05, fold-regulation >2, and mean base >20 are displayed. See Table S2 for the complete, annotated gene list with IP-association, respective CDs and statistics. The sGCA script and MATLAB app are available on GitHub (https://github.com/niethamp/sGCA-Ma-et-al.-2022-)

QUANTIFICATION AND STATISTICAL ANALYSIS

The error bars in neutrophil or macrophage tracking during 2-h PA ear infection indicate standard errors of means (SEM), other error bars indicate standard deviation (STDEV). For most mean value comparisons, p values were derived by student's t-test (two tailed, two sample unequal variance test, heteroscedastic) using Prism (GraphPad) or Excel (Microsoft). For comparison of Kaplan-Meier survival curves, a log rank (Mantel-Cox) test in Prism was used. For statistical analysis, animal experiments from different experimental days were aggregated. Sample sizes were not predetermined by statistical methods. The experiments were not randomized, and the investigators were not blinded to allocation during experiments or outcome assessment.

Supplementary Material

Refer to Web version on PubMed Central for supplementary material.

ACKNOWLEDGMENTS

REFERENCES

1. Shay T, Jojic V, Zuk O, Rothamel K, Puyraimond-Zemmour D, Feng T, Wakamatsu E, Benoist C, Koller D, Regev A, et al. (2013). Conservation and divergence in the transcriptional programs of the human and mouse immune systems. Proc. Natl. Acad. Sci. USA 110, 2946–2951. 10.1073/pnas.1222738110. [PubMed: 23382184]

2. Seok J, Warren HS, Cuenca AG, Mindrinos MN, Baker HV, Xu W, Richards DR, McDonald-Smith GP, Gao H, Hennessy L, et al. (2013). Genomic responses in mouse models poorly mimic human inflammatory diseases. Proc. Natl. Acad. Sci. USA 110, 3507–3512. 10.1073/pnas.1222878110. [PubMed: 23401516]

3. Powell WS, and Rokach J (2020). Targeting the OXE receptor as a potential novel therapy for asthma. Biochem. Pharmacol. 179, 113930. 10.1016/j.bcp.2020.113930. [PubMed: 32240653]

4. Powell WS, and Rokach J (2013). The eosinophil chemoattractant 5-oxo-ETE and the OXE receptor. Prog. Lipid Res. 52, 651–665. 10.1016/j.plipres.2013.09.001. [PubMed: 24056189]

5. Farias SE, Basselin M, Chang L, Heidenreich KA, Rapoport SI, and Murphy RC (2008). Formation of eicosanoids, E2/D2 isoprostanes, and docosanoids following decapitation-induced ischemia, measured in high-energy-microwaved rat brain. J. Lipid Res. 49, 1990–2000. 10.1194/jlr.M800200-JLR200. [PubMed: 18503030]

6. Kowal K, Gielicz A, and Sanak M (2017). The effect of allergen-induced bronchoconstriction on concentration of 5-oxo-ETE in exhaled breath condensate of house dust mite-allergic patients. Clin. Exp. Allergy 47, 1253–1262. 10.1111/cea.12990. [PubMed: 28763131]

7. Miller LA, Cossette C, Chourey S, Ye Q, Reddy CN, Rokach J, and Powell WS (2020). Inhibition of allergen-induced dermal eosinophilia by an oxoeicosanoid receptor antagonist in non-human primates. Br. J. Pharmacol. 177, 360–371. 10.1111/bph.14872. [PubMed: 31655023]

8. Cossette C, Miller LA, Ye Q, Chourey S, Reddy CN, Rokach J, and Powell WS (2022). Targeting the OXE receptor with a selective antagonist inhibits allergen-induced pulmonary inflammation in non-human primates. Br. J. Pharmacol. 179, 322–336. 10.1111/bph.15721. [PubMed: 34766334]

9. Gao J, Aksoy BA, Dogrusoz U, Dresdner G, Gross B, Sumer SO, Sun Y, Jacobsen A, Sinha R, Larsson E, et al. (2013). Integrative analysis of complex cancer genomics and clinical profiles using the cBioPortal. Sci. Signal. 6, pl1. 10.1126/scisignal.2004088. [PubMed: 23550210]

10. Sundaram S, and Ghosh J (2006). Expression of 5-oxoETE receptor in prostate cancer cells: critical role in survival. Biochem. Biophys. Res. Commun. 339, 93–98. 10.1016/j.bbrc.2005.10.189. [PubMed: 16289380]

11. O'Flaherty JT, Rogers LC, Paumi CM, Hantgan RR, Thomas LR, Clay CE, High K, Chen YQ, Willingham MC, Smitherman PK, et al. (2005). 5-Oxo-ETE analogs and the proliferation of cancer cells. Biochim. Biophys. Acta 1736, 228–236. 10.1016/j.bbalip.2005.08.009. [PubMed: 16154383]

12. Enyedi B, Kala S, Nikolich-Zugich T, and Niethammer P (2013). Tissue damage detection by osmotic surveillance. Nat. Cell Biol. 15, 1123–1130. 10.1038/ncb2818. [PubMed: 23934216]

13. Robertson TF, and Huttenlocher A (2022). Real-time imaging of inflammation and its resolution: it's apparent because it's transparent. Immunol. Rev. 306, 258–270. 10.1111/imr.13061. [PubMed: 35023170]

14. Trede NS, Langenau DM, Traver D, Look AT, and Zon LI (2004). The use of zebrafish to understand immunity. Immunity 20, 367–379. 10.1016/s1074-7613(04)00084-6. [PubMed: 15084267]

15. Stamatiou P, Hamid Q, Taha R, Yu W, Issekutz TB, Rokach J, Khanapure SP, and Powell WS (1998). 5-oxo-ETE induces pulmonary eosinophilia in an integrin-dependent manner in Brown Norway rats. J. Clin. Invest. 102, 2165–2172. 10.1172/JCI1995. [PubMed: 9854052]

16. Almishri W, Cossette C, Rokach J, Martin JG, Hamid Q, and Powell WS (2005). Effects of prostaglandin D2, 15-deoxy-Delta12, 14-prostaglandin J2, and selective DP1 and DP2 receptor agonists on pulmonary infiltration of eosinophils in Brown Norway rats. J. Pharmacol. Exp. Ther. 313, 64–69. 10.1124/jpet.104.079079. [PubMed: 15590767]

17. MacLeod AS, and Mansbridge JN (2016). The innate immune system in acute and chronic wounds. Adv. Wound Care 5, 65–78. 10.1089/wound.2014.0608.

18. Mercier F, Morin C, Cloutier M, Proteau S, Rokach J, Powell WS, and Rousseau E (2004). 5-Oxo-ETE regulates tone of Guinea pig airway smooth muscle via activation of Ca2+ pools and Rho-kinase pathway. Am. J. Physiol. Lung Cell Mol. Physiol. 287, L631–L640. 10.1152/ajplung.00005.2004. [PubMed: 15090369]

19. Maus KD, Stephenson DJ, Ali AN, MacKnight HP, Huang H-J, Serrats J, Kim M, Diegelmann RF, and Chalfant CE (2022). Ceramide kinase regulates acute wound healing by suppressing 5-oxo-ETE biosynthesis and signaling via its receptor OXER1. J. Lipid Res. 63, 100187. 10.1016/j.jlr.2022.100187. [PubMed: 35219746]

20. Hu Y, Flockhart I, Vinayagam A, Bergwitz C, Berger B, Perrimon N, and Mohr SE (2011). An integrative approach to ortholog prediction for disease-focused and other functional studies. BMC Bioinformatics 12, 357. 10.1186/1471-2105-12-357. [PubMed: 21880147]

21. Farnsworth DR, Saunders LM, and Miller AC (2020). A single-cell transcriptome atlas for zebrafish development. Dev. Biol. 459, 100–108. 10.1016/j.ydbio.2019.11.008. [PubMed: 31782996]

22. Deng Q, Harvie EA, and Huttenlocher A (2012). Distinct signalling mechanisms mediate neutrophil attraction to bacterial infection and tissue injury. Cell Microbiol. 14, 517–528. 10.1111/j.1462-5822.2011.01738.x. [PubMed: 22188170]

23. Deng Q, Sarris M, Bennin DA, Green JM, Herbomel P, and Huttenlocher A (2013). Localized bacterial infection induces systemic activation of neutrophils through Cxcr2 signaling in zebrafish. J. Leukoc. Biol. 93, 761–769. 10.1189/jlb.1012534. [PubMed: 23475575]

24. Huang C, and Niethammer P (2018). Tissue damage signaling is a prerequisite for protective neutrophil recruitment to microbial infection in zebrafish. Immunity 48, 1006–1013.e6. 10.1016/j.immuni.2018.04.020. [PubMed: 29768163]

25. Quehenberger O, Armando AM, Brown AH, Milne SB, Myers DS, Merrill AH, Bandyopadhyay S, Jones KN, Kelly S, Shaner RL, et al. (2010). Lipidomics reveals a remarkable diversity of lipids in human plasma. J. Lipid Res. 51, 3299–3305. 10.1194/jlr.M009449. [PubMed: 20671299]

26. Powell WS, Gravel S, MacLeod RJ, Mills E, and Hashefi M (1993). Stimulation of human neutrophils by 5-oxo-6, 8, 11, 14-eicosatetraenoic acid by a mechanism independent of the leukotriene B4 receptor. J. Biol. Chem. 268, 9280–9286. 10.1016/S0021-9258(18)98347-X. [PubMed: 8387490]

27. Enyedi B, Jelcic M, and Niethammer P (2016). The cell nucleus serves as a mechanotransducer of tissue damage-induced inflammation. Cell 165, 1160–1170. 10.1016/j.cell.2016.04.016. [PubMed: 27203112]

28. Benard EL, van der Sar AM, Ellett F, Lieschke GJ, Spaink HP, and Meijer AH (2012). Infection of zebrafish embryos with intracellular bacterial pathogens. J. Vis. Exp. 61, 3781. 10.3791/3781.

29. Hoshijima K, Jurynec MJ, Klatt Shaw D, Jacobi AM, Behlke MA, and Grunwald DJ (2019). Highly efficient CRISPR-Cas9-based methods for generating deletion mutations and F0 embryos that lack gene function in zebrafish. Dev. Cell 51, 645–657.e4. 10.1016/j.devcel.2019.10.004. [PubMed: 31708433]

30. Wu RS, Lam II, Clay H, Duong DN, Deo RC, and Coughlin SR (2018). A rapid method for directed gene knockout for screening in G0 zebrafish. Dev. Cell 46, 112–125.e4. 10.1016/j.devcel.2018.06.003. [PubMed: 29974860]

31. Erlemann K-R, Cossette C, Gravel S, Lesimple A, Lee G-J, Saha G, Rokach J, and Powell WS (2007). Airway epithelial cells synthesize the lipid mediator 5-oxo-ETE in response to oxidative stress. Free Radic. Biol. Med. 42, 654–664. 10.1016/j.freeradbiomed.2006.12.006. [PubMed: 17291989]

32. Erlemann K-R, Rokach J, and Powell WS (2004). Oxidative stress stimulates the synthesis of the eosinophil chemoattractant 5-oxo-6, 8, 11, 14-eicosatetraenoic acid by inflammatory cells. J. Biol. Chem. 279, 40376–40384. 10.1074/jbc.M401294200. [PubMed: 15234979]

33. Sun Y, Karmakar M, Roy S, Ramadan RT, Williams SR, Howell S, Shive CL, Han Y, Stopford CM, Rietsch A, et al. (2010). TLR4 and TLR5 on corneal macrophages regulate Pseudomonas aeruginosa keratitis by signaling through MyD88-dependent and -independent pathways. J. Immunol. 185, 4272–4283. 10.4049/jimmunol.1000874. [PubMed: 20826748]

34. Alhazmi A (2018). NOD-like receptor(s) and host immune responses with Pseudomonas aeruginosa infection. Inflamm. Res. 67, 479–493. 10.1007/s00011-018-1132-0. [PubMed: 29353310]

35. Lämmermann T, Afonso PV, Angermann BR, Wang JM, Kastenmüller W, Parent CA, and Germain RN (2013). Neutrophil swarms require LTB4 and integrins at sites of cell death in vivo. Nature 498, 371–375. 10.1038/nature12175. [PubMed: 23708969]

36. Poplimont H, Georgantzoglou A, Boulch M, Walker HA, Coombs C, Papaleonidopoulou F, and Sarris M (2020). Neutrophil swarming in damaged tissue is orchestrated by connexins and cooperative calcium alarm signals. Curr. Biol. 30, 2761–2776.e7. 10.1016/j.cub.2020.05.030. [PubMed: 32502410]

37. Isles HM, Loynes CA, Alasmari S, Kon FC, Henry KM, Kadochnikova A, Hales J, Muir CF, Keightley M-C, Kadirkamanathan V, et al. (2021). Pioneer neutrophils release chromatin within in vivo swarms. Elife 10, e68755. 10.7554/eLife.68755. [PubMed: 34292151]

38. de Oliveira S, Boudinot P, Calado Â, and Mulero V (2015). Duox1-derived H2O2 modulates Cxcl8 expression and neutrophil recruitment via JNK/c-JUN/AP-1 signaling and chromatin modifications. J. Immunol. 194, 1523–1533. 10.4049/jimmunol.1402386. [PubMed: 25582859]

39. Bhatt L, Roinestad K, Van T, and Springman EB (2017). Recent advances in clinical development of leukotriene B4 pathway drugs. Semin. Immunol. 33, 65–73. 10.1016/j.smim.2017.08.007. [PubMed: 29042030]

40. Zhou Q, Yang D, Ombrello AK, Zavialov AV, Toro C, Zavialov AV, Stone DL, Chae JJ, Rosenzweig SD, Bishop K, et al. (2014). Early-onset stroke and vasculopathy associated with

mutations in ADA2. N. Engl. J. Med. 370, 911–920. 10.1056/NEJMoa1307361. [PubMed: 24552284]

41. White RM, Sessa A, Burke C, Bowman T, LeBlanc J, Ceol C, Bourque C, Dovey M, Goessling W, Burns CE, et al. (2008). Transparent adult zebrafish as a tool for in vivo transplantation analysis. Cell Stem Cell 2, 183–189. 10.1016/j.stem.2007.11.002. [PubMed: 18371439]

42. Stoddard M, Huang C, Enyedi B, and Niethammer P (2019). Live imaging of leukocyte recruitment in a zebrafish model of chemical liver injury. Sci. Rep. 9, 28. 10.1038/s41598-018-36771-9. [PubMed: 30631093]

43. Cunliffe VT (2003). Zebrafish: a practical approach. Edited by NÜSSLEIN-VOLHARD C and DAHM R. Oxford university press. 2002. 322 pages. ISBN 0 19 963808 X. Price £40.00 (paperback). ISBN 0 19 963809 8. Price £80.00 (hardback). Genet. Res. 82, 79. 10.1017/S0016672303216384.

44. Bolcome RE, Sullivan SE, Zeller R, Barker AP, Collier RJ, and Chan J (2008). Anthrax lethal toxin induces cell death-independent permeability in zebrafish vasculature. Proc. Natl. Acad. Sci. USA 105, 2439–2444. 10.1073/pnas.0712195105. [PubMed: 18268319]

45. Miskolci V, Squirrell J, Rindy J, Vincent W, Sauer JD, Gibson A, Eliceiri KW, and Huttenlocher A (2019). Distinct inflammatory and wound healing responses to complex caudal fin injuries of larval zebrafish. Elife 8, e45976. 10.7554/eLife.45976. [PubMed: 31259685]

46. Rosowski EE, Raffa N, Knox BP, Golenberg N, Keller NP, and Huttenlocher A (2018). Macrophages inhibit Aspergillus fumigatus germination and neutrophil-mediated fungal killing. PLoS Pathog. 14, e1007229. 10.1371/journal.ppat.1007229. [PubMed: 30071103]

47. Katikaneni A, Jelcic M, Gerlach GF, Ma Y, Overholtzer M, and Niethammer P (2020). Lipid peroxidation regulates long-range wound detection through 5-lipoxygenase in zebrafish. Nat. Cell Biol. 22, 1049–1055. 10.1038/s41556-020-0564-2. [PubMed: 32868902]

48. Astin JW, Keerthisinghe P, Du L, Sanderson LE, Crosier KE, Crosier PS, and Hall CJ (2017). Innate immune cells and bacterial infection in zebrafish. Methods Cell Biol. 138, 31–60. 10.1016/bs.mcb.2016.08.002. [PubMed: 28129850]

49. Bertrand JY, Kim AD, Violette EP, Stachura DL, Cisson JL, and Traver D (2007). Definitive hematopoiesis initiates through a committed erythromyeloid progenitor in the zebrafish embryo. Development 134, 4147–4156. 10.1242/dev.012385. [PubMed: 17959717]

50. Livak KJ, and Schmittgen TD (2001). Analysis of relative gene expression data using real-time quantitative PCR and the 2(-Delta Delta C(T)) Method. Methods 25, 402–408. 10.1006/meth.2001.1262. [PubMed: 11846609]

Highlights

- 5-oxoETE and its receptor OXER1 are induced by bacterial infection

- OXER1 orthologs are present in fish and humans but absent in popular rodent models

- OXER1's innate immune functions are illuminated in the zebrafish model
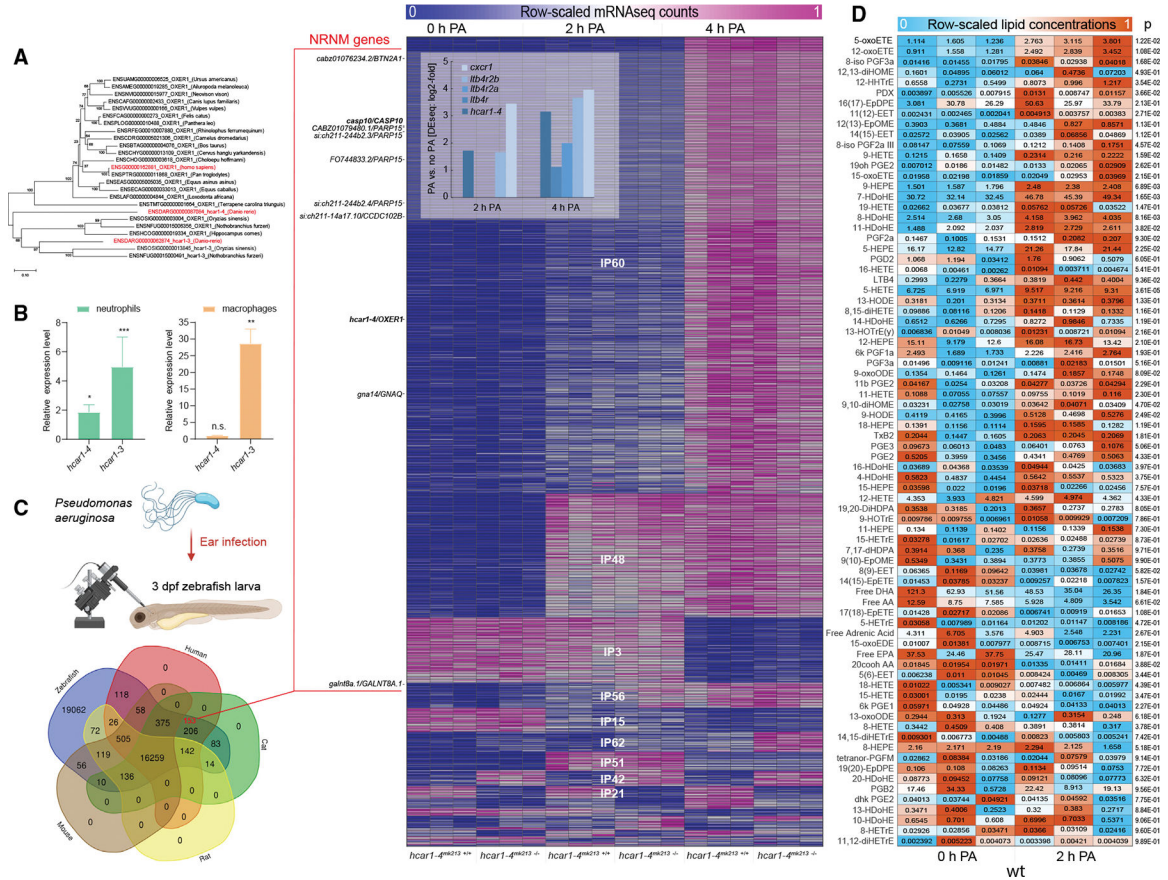
Figure 1. The 5-oxoETE pathway is induced by ear infection of zebrafish larvae with *P. aeruginosa*

(A) OXER1 phylogenetic tree.

(B) Relative expression levels of *hcar1–3* and *hcar1–4* mRNA in leukocytes compared with the rest of the body determined by FACS-sorting of dissociated neutrophil (left panel, TG(*lyz*:pm2-mk2)) or macrophage (right panel, TG(*mpeg1: eGFP*)) reporter zebrafish larvae and qRT-PCR. Error bars, SD of three different pools of zebrafish leukocytes. *p < 0.05, **p < 0.01, ***p < 0.001, n.s., p > 0.05; Student's t test (two tailed, two sample unequal variance test).

(C) Top left panel: experimental cartoon scheme. This figure was created with BioRender. Bottom left panel: Venn diagram of zebrafish genes with ENSEMBL orthologs (ENSEMBL release 107) in human, cat, mouse, and rat. Red number, number of DIOPT-filtered NRNM genes (see STAR Methods). Right panel: sorted sGCA heatmap of significantly regulated mRNA-seq expression profiles (fold-regulation > 2, p$_{adj}$ < 0.05 by Benjamini and Hochberg method) with high similarity to the respective binary expression phenotypes (correlation distance < 0.25, Figure S1B, also see STAR Methods and MATLAB sGCA script). Color scale, mRNA-seq profiles are row-scaled between 0 (blue) and 1 (pink). Shown are three biological replicates per experimental condition. Heatmap inset: significant (p$_{adj}$ < 0.05) fold-upregulation of select inflammatory receptor mRNAs 2 and 4 h after PA infection as calculated by DEseq2. DIOPT-filtered NRNM genes are marked on the left side of the

heatmap (zebrafish gene/human ortholog). NRNM genes with "high"-ranked (criteria see STAR Methods) human orthologs are printed in bold.

(D) Heatmap of row-scaled lipid concentrations as measured by LIPIDMAPS full panel eicosanoid mass spectroscopical analysis. Color scale, relative lipid concentrations are row-scaled between 0 (blue) and 1 (orange). Boxed numbers, absolute lipid concentrations in pmol/mg tissue (~μM). Note that the color scale does not represent these absolute lipid concentrations, but that it highlights the relative changes for each lipid. Shown are three biological replicates (i.e., ~400 3 dpf zebrafish larvae per pool) per experimental condition. Numbers right of heatmap, p values of Student's t test (two tailed, two sample unequal variance test) comparing 0 h PA vs. 2 h PA.

See also Figure S1 and Tables S1 and S2.
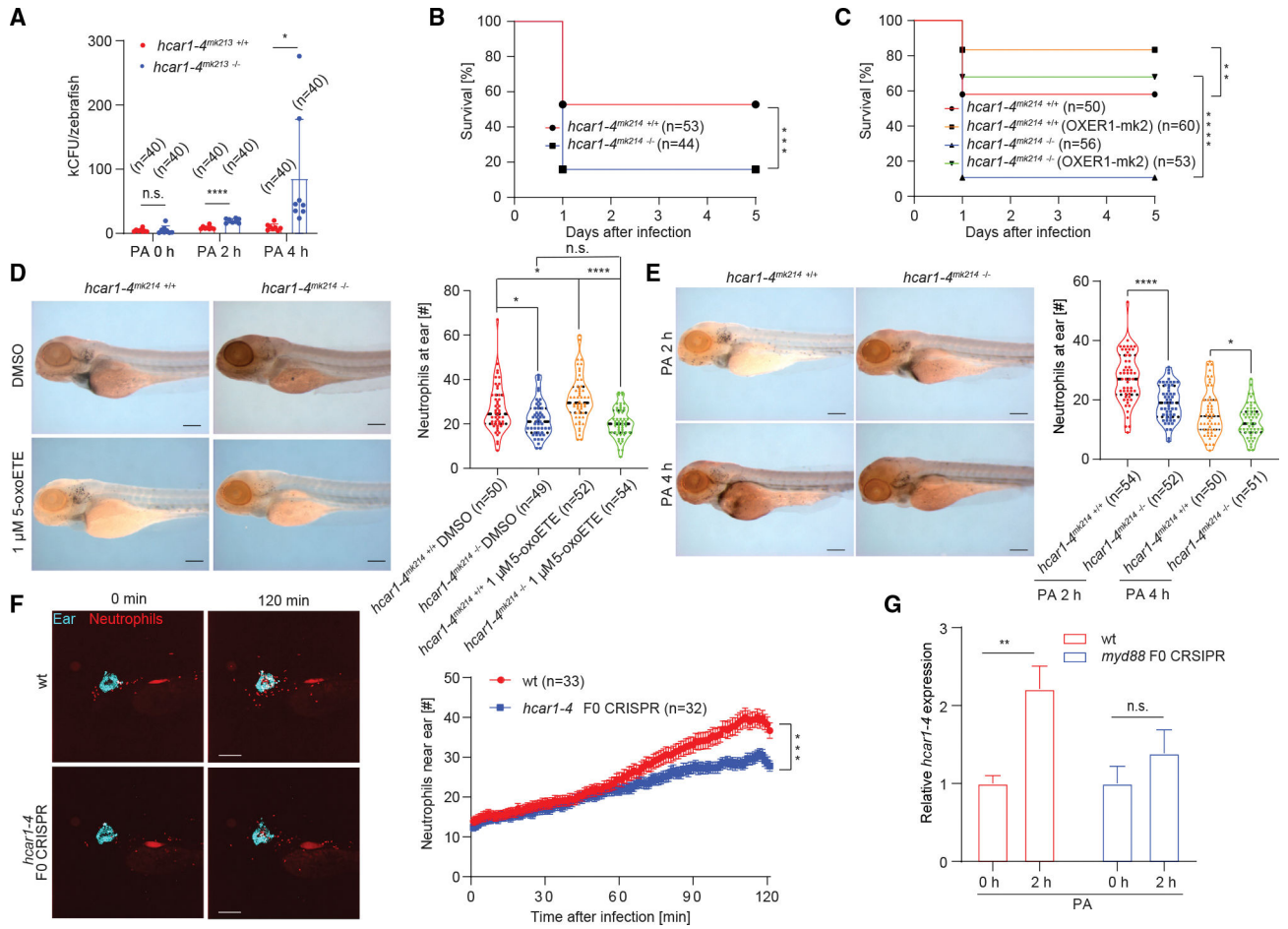
Figure 2. The 5-oxoETE pathway mediates early antimicrobial neutrophil recruitment to infection sites

(A) Colony forming units (CFU) per infected larvae at indicated times after infection. *p < 0.05; ****p < 0.00001; Student's t test (two tailed, two sample unequal variance test). Error bars, SD of eight independently infected zebrafish pools (five larvae per group) comprising a total of n = 40 larvae per pool.

(B and C) Meier-Kaplan survival plots of PA-infected *hcar1–4$^{mk214 +/+}$* (WT) and *hcar1–4$^{mk214 -/-}$* larvae without (B) or with (C) ectopic expression of human OXER1 fused with mKate2 (OXER1-mk2). **p < 0.01; ***p < 0.001; ****p < 0.0001; log rank test. Parentheses, number of injected larvae per group.

(D) 5-oxoETE-dependent neutrophil recruitment to infected ears requires *hcar1–4*. Larvae were injected with PA mixed with pure 5-oxoETE (in DMSO) or DMSO alone as vehicle control. During infection and incubation, the larvae were kept under isotonic bathing conditions (Iso E3) to suppress osmotic tissue damage signals as previously described in Huang and Niethammer, 2018.[24] Left panel, representative images of Sudan-black-stained neutrophils at the infected ears of WT and *hcar1–4$^{mk214 -/-}$* larvae 2 h after ear injection. Scale bar, 200 μm. Right panel, quantification of neutrophil counts at the ears at the indicated times after infection. Violin plots lines denote first quartiles (top line), medians (middle line), third quartiles (bottom line). Violin plot points denote neutrophil counts in

individual larvae. *p < 0.05; ****p < 0.0001; n.s., p > 0.05; Student's t test (two tailed, two sample unequal variance test). N, total number of injected larvae per condition.

(E) Left panel: representative images of Sudan-black-staining of neutrophils at the infected ears of WT and *hcar1–4*^{mk214 –/–} larvae. Scale bar, 200 μm. Right panel: quantification of neutrophil recruitment to the ears at the indicated times after infection. Violin plots lines denote first quartiles (top line), medians (middle line), and third quartiles (bottom line). Violin plot points denote neutrophil counts in individual larvae. *p < 0.05; ****p < 0.0001; Student's t test (two tailed, two sample unequal variance test). Parentheses, total number of injected larvae.

(F) Live imaging of neutrophil recruitment to ear in WT and *hcar1–4* F0 CRISPR larvae (TG(*lyz*:pm2-mk2) background). Left panel: representative time-lapse images at indicated times after infection. Cyan, fluorescent beads co-injected with PA into the ear. Red, mKate2-expressing neutrophils. Scale bar, 200 μm. Right panel: neutrophil number in a 390 μm × 390 μm × 100 μm box around the ear counted by 3D segmentation of confocal imaging stacks. Error bar, SEM of n infected WT (red) or F0 CRSIPR (blue) larvae. ***p < 0.001; Student's t test (two tailed, two sample unequal variance test) applied to the final time point (t = 120 min).

(G) Relative mRNA expression levels of *hcar1–4* at 2 h after PA ear infection as measured by qRT-PCR in 3 dpf zebrafish larvae (WT and *myd88* F0 CRISPR). Actin was used as an internal control. Error bars, SD of three different pools of zebrafish larvae. **p < 0.01; n.s., p > 0.05; Student's t test (two tailed, two sample unequal variance test).

See also Figures S2 and S3.
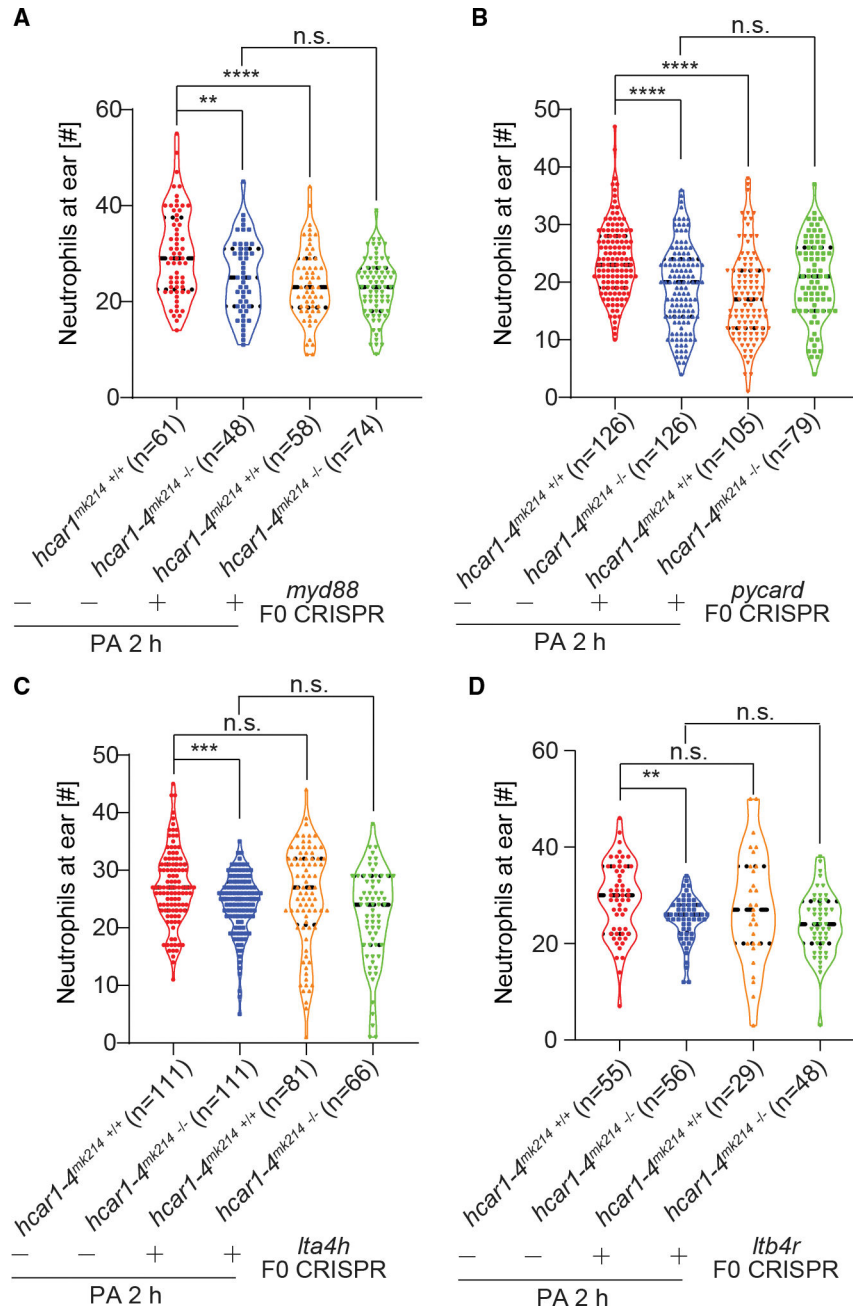
Figure 3. Oxoeicosanoid and not LTB$_4$ signaling regulates early neutrophil recruitment along with microbial pattern recognition

(A and B) *Myd88* and *pycard* mutations (F0 CRISPR) inhibit early neutrophil recruitment to infected ears to a similar extent as *hcar1–4*$^{mk214\,-/-}$ mutation does but without having an additive effect to the latter.

(C and D) Unlike the *hcar1–4*$^{mk214\,-/-}$ mutation, *lta4h* and *ltb4r* F0 CRISPR mutations do not inhibit early neutrophil recruitment to infected ears. Violin plot points denote counts of Sudan-black-stained neutrophils in individual larvae. Violin plots lines denote first quartiles (top line), medians (middle line), and third quartiles (bottom line). **p < 0.01; ***p < 0.001;
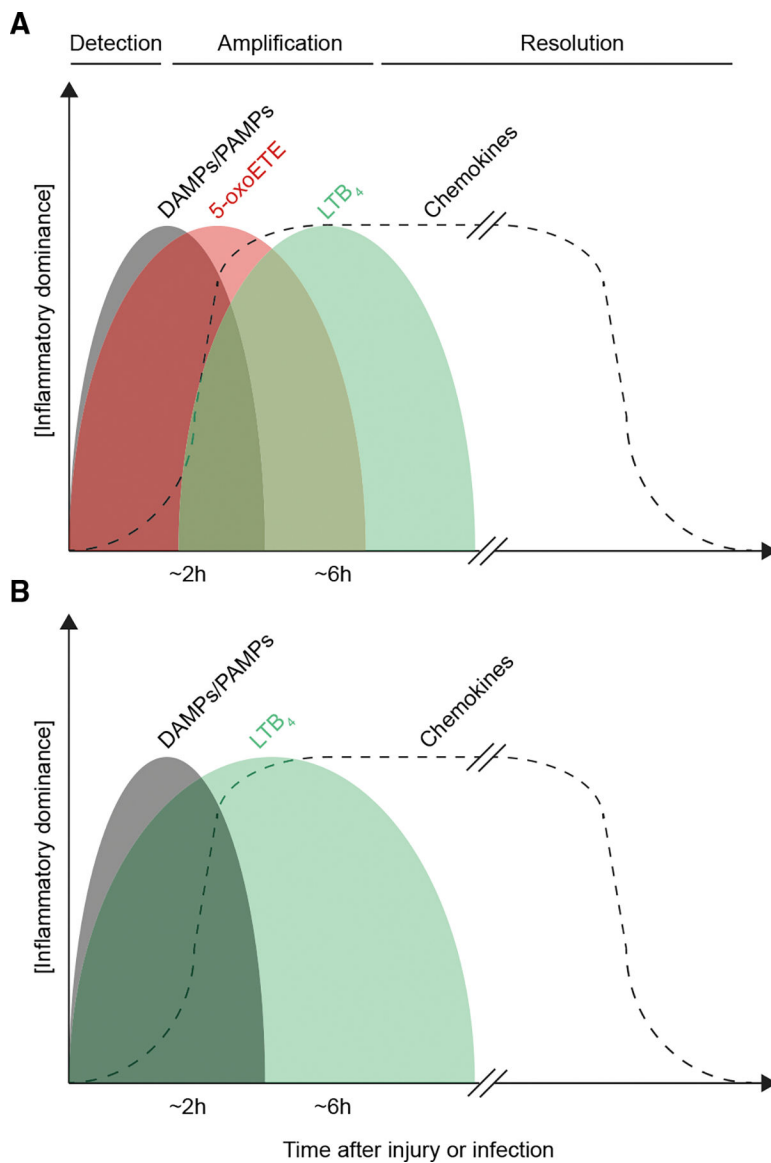
****p < 0.0001; n.s., p > 0.05; Student's t test (two tailed, two sample unequal variance test). Parentheses, total number of injected larvae.

See also Figure S4.

Figure 4. Hypothetical scheme of inflammatory mediator sequence after injury and infection
Hypothetical cartoon scheme of approximate regulatory timelines in (A) non-rodent and (B) rodent inflammation. DAMPs, damage associated molecular patterns. PAMPs, pathogen associated molecular patterns.

KEY RESOURCES TABLE

REAGENT or RESOURCE	SOURCE	IDENTIFIER
Bacterial and virus strains		
Wt PA14	Joao Xavier (MSKCC)	N/A
Chemicals, peptides, and recombinant proteins		
Blue-green (Cyan) fluorescent beads (Ex/Em=430/465)	Thermo Fisher	Cat#F13080
Red fluorescent beads (Ex/Em=580/605)	Thermo Fisher	Cat#F8810
Dextran, Fluorescein, 500,000 MW, Anionic, Lysine Fixable	Invitrogen	Cat#D7136
Agarose LM	Gold Biotechnology	Cat#A-204-100
5-oxoETE	Cayman	Cat#34250
Dimethyl sulfoxide (DMSO)	Sigma	Cat#D8418
ethyl 3-aminobenzoate methanesulfonate (Tricaine)	Sigma	Cat#E10521
Triton X-100	Sigma	Cat#SLBW7103
Phosphate buffered saline (PBS)	Sigma	Cat#79382
FastDigest NotI restriction enzyme	Thermo Fisher	Cat#FD0593
FastDigest BstXI restriction enzyme	Thermo Fisher	Cat#FD1024
FastDigest BseLI restriction enzyme	Thermo Fisher	Cat#FD1204
FastDigest MseI (Tru1I) restriction enzyme	Thermo Fisher	Cat#ER0981
FastDigest BseNI restriction enzyme	Thermo Fisher	Cat#FD0884
FastDigest HpaII restriction enzyme	Thermo Fisher	Cat#FD0514
FastDigest Eco47I restriction enzyme	Thermo Fisher	Cat#FD0314
FastDigest OliI restriction enzyme	Thermo Fisher	Cat#FD1634
FastDigest PvuI restriction enzyme	Thermo Fisher	Cat#FD0624
FastDigest Bsp1286I (SduI) restriction enzyme	Thermo Fisher	Cat#FD0654
FastDigest SmlI (SmoI) restriction enzyme	Thermo Fisher	Cat#ER1981
FastDigest SalI restriction enzyme	Thermo Fisher	Cat#FD0644
Critical commercial assays		
mMessage mMachine SP6 Kit	Thermo Fisher	Cat#AM1340
Trizol reagent	Thermo Fisher	Cat#15596026
RevertAid First Strand cDNA Synthesis Kit	Thermo Fisher	Cat#K1621
RNeasy Plus Micro kit	QIAGEN	Cat#74034
High-Capacity cDNA Reverse Transcript Kit	Thermo Fisher	Cat#4368814
Maxima SYBR Green/Fluorescein qPCR Master Mix	Thermo Fisher	Cat#K0242
Deposited data		
RNA-seq	This paper	GSE201604
Code	This paper	https://doi.org/10.5281/zenodo.7419586

REAGENT or RESOURCE	SOURCE	IDENTIFIER
Experimental models: Organisms/strains		
Zebrafish: wt *casper*	White et al., 2008[41]	https://doi.org/10.1016/j.stem.2007.11.002
Zebrafish: TG(*lyz*:pm2-mk2)	Stoddard et al., 2019[42]	https://doi.org/10.1038/s41598-018-36771-9
Zebrafish: TG(*mpeg1*:eGFP)	Stoddard et al., 2019[42]	https://doi.org/10.1038/s41598-018-36771-9
Zebrafish: *hcar1–4*$^{mk213\ +/+}$	This paper	N/A
Zebrafish: *hcar1–4*$^{mk213\ -/-}$	This paper	N/A
Zebrafish: *hcar1–4*$^{mk214\ +/+}$	This paper	N/A
Zebrafish: *hcar1–4*$^{mk214\ -/-}$	This paper	N/A
Oligonucleotides		
See Table S3 for Oligonucleotides	This paper	N/A
Software and algorithms		
ImageJ/FIJI (ImageJ 1.53t, v2.9.0.)	Johannes Schindelin	https://fiji.sc/
MATLAB (9.12.0.1975300 (R2022a) Update 3)	Mathworks Inc., USA	http://mathworks.com
Bioinformatics Toolbox Version 4.16 (R2022a)	Mathworks Inc., USA	http://mathworks.com
Computer Vision Toolbox Version 10.2 (R2022a)	Mathworks Inc., USA	http://mathworks.com
Curve Fitting Toolbox Version 3.7 (R2022a)	Mathworks Inc., USA	http://mathworks.com
Deep Learning Toolbox Version 14.4 (R2022a)	Mathworks Inc., USA	http://mathworks.com
Fuzzy Logic Toolbox Version 2.9 (R2022a)	Mathworks Inc., USA	http://mathworks.com
Global Optimization Toolbox Version 4.7 (R2022a)	Mathworks Inc., USA	http://mathworks.com
Image Processing Toolbox Version 11.5 (R2022a)	Mathworks Inc., USA	http://mathworks.com
MATLAB Compiler Version 8.4 (R2022a)	Mathworks Inc., USA	http://mathworks.com
Mapping Toolbox Version 5.3 (R2022a)	Mathworks Inc., USA	http://mathworks.com
Optimization Toolbox Version 9.3 (R2022a)	Mathworks Inc., USA	http://mathworks.com
Parallel Computing Toolbox Version 7.6 (R2022a)	Mathworks Inc., USA	http://mathworks.com
Partial Differential Equation Toolbox Version 3.8 (R2022a)	Mathworks Inc., USA	http://mathworks.com
Sensor Fusion and Tracking Toolbox (R2022a)	Mathworks Inc., USA Version 2.3	http://mathworks.com
Signal Processing Toolbox Version 9.0 (R2022a)	Mathworks Inc., USA	http://mathworks.com
Statistics and Machine Learning Toolbox Version 12.3 (R2022a)	Mathworks Inc., USA	http://mathworks.com
NIS imaging software (Nikon, v5.11.01)	Nikon Microscope Product	https://www.microscope.healthcare.nikon.com/products/software/nis-elements
Prism (GraphPad, v8.3.0)	GraphPad Software	https://www.graphpad.com/scientific-software/prism
Imaris (Bitplane, v9.6.0)	Molecular Cytology Core Facility at MSKCC	https://imaris.oxinst.com/